

# Steady subsidence of a repeatedly erupting caldera through InSAR observations: Aso, Japan

Adriano Nobile<sup>1</sup>  · Valerio Acocella<sup>2</sup> · Joel Ruch<sup>3</sup> · Yosuke Aoki<sup>4</sup> · Sven Borgstrom<sup>5</sup> · Valeria Siniscalchi<sup>5</sup> · Nobuo Geshi<sup>6</sup>

Received: 21 July 2016 / Accepted: 14 March 2017 / Published online: 5 April 2017  
© Springer-Verlag Berlin Heidelberg 2017

**Abstract** The relation between unrest and eruption at calderas is still poorly understood. Aso caldera, Japan, shows minor episodic phreatomagmatic eruptions associated with steady subsidence. We analyse the deformation of Aso using SAR images from 1993 to 2011 and compare it with the eruptive activity. Although the dataset suffers from limitations (e.g. atmospheric effects, coherence loss, low signal-to-noise ratio), we observe a steady subsidence signal from 1996 to 1998, which suggests an overall contraction of a magmatic source below the caldera centre, from 4 to 5 km depth. We propose that the observed contraction may have been induced by the release of the magmatic fluids feeding the eruptions. If confirmed by further data, this hypothesis suggests that degassing processes play a crucial role in triggering minor eruptions within open conduit calderas, such as at Aso. Our study

underlines the importance of defining any eruptive potential also from deflating magmatic systems with open conduit.

**Keywords** Calderas · Subsidence · Magmatic source · InSAR · Outgassing · Aso

## Introduction

Calderas are the surface expression of long-lived and complex magmatic systems, often associated with shallower hydrothermal systems. All monitored calderas have experienced unrest, defined as a deviation from the quiescent state of a volcano and expressed as variations in the geodetic, seismic and degassing monitoring parameters, which may culminate in an eruption. Some felsic calderas have experienced continuous unrest for decades or centuries, exhibiting restless behaviour (e.g. Newhall and Dzurisin 1988). Understanding the relation between unrest and eruption at active calderas is crucial for forecasting volcanic activity and evaluating the related hazard. This relation is still poorly understood, however, because monitoring data acquired during unrest do not necessarily provide unequivocal information on the state of the shallow magmatic system. For example, pre-eruptive unrest at calderas is usually characterized by uplift (e.g. Newhall and Dzurisin 1988; Acocella et al. 2015), but there are cases where repeated eruptions have been preceded by subsidence, such as at Aso caldera, Japan (Figs. 1 and 2b). Aso has experienced repeated minor eruptions in an overall context of subsidence, which has lasted for several decades (Sudo et al. 2006). This unexpected behaviour highlights a worrisome shortfall in correctly understanding the unrest signals (in this case the surface deformation), which possibly precede eruptions and which could potentially allow assessment of volcanic hazard.

To better define the features of these recent eruptions, as well as to understand the processes involved, we use synthetic aperture

---

Editorial responsibility: K.V. Cashman

---

**Electronic supplementary material** The online version of this article (doi:10.1007/s00445-017-1112-1) contains supplementary material, which is available to authorized users.

---

✉ Adriano Nobile  
adriano.nobile@africamuseum.be

<sup>1</sup> Royal Museum for Central Africa, Leuvenesteenweg 13, 3080 Tervuren, Belgium

<sup>2</sup> Dipartimento Scienze Università Roma Tre, Rome, Italy

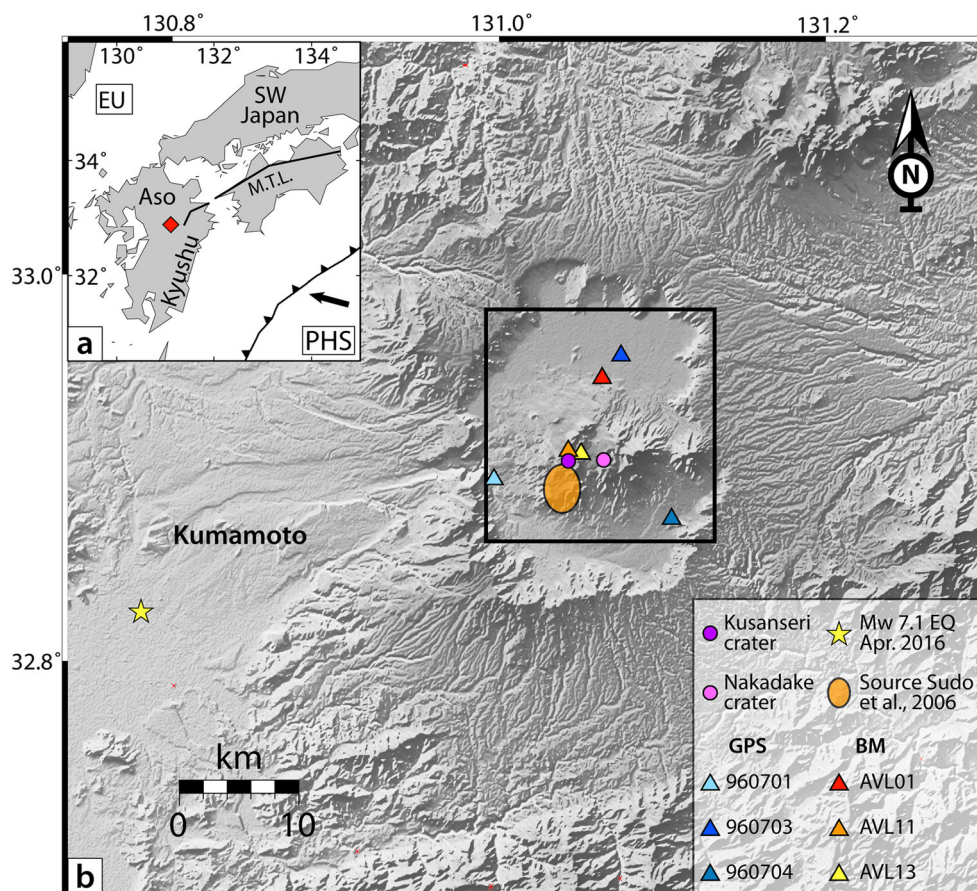
<sup>3</sup> King Abdullah University of Science and Technology, Jeddah, Saudi Arabia

<sup>4</sup> Earthquake Research Institute—The University of Tokyo, Tokyo, Japan

<sup>5</sup> INGV—Osservatorio Vesuviano, Naples, Italy

<sup>6</sup> Geological Survey Japan, AIST, Tsukuba, Ibaraki, Japan

**Fig. 1** **a** SW Japan, Kyushu Island and Aso Caldera (*red diamond*). *M.T.L.* Median Tectonic Line, *PHS* Philippine Sea plate, *EU* Eurasian plate. **b** Aso Caldera SRTM Digital Elevation Model. *Pink circle* = Nakadake crater, *violet circle* = Kusasenri crater. *Triangles* are GPS stations (Geospatial Information Authority 2011) and levelling benchmarks (Sudo et al. 2006). *Orange ellipse* locates deformation source for 1997–2004 of Sudo et al. (2006). *Yellow star* is USGS location for the Mw 7.1, 16 April 2016 Kumamoto earthquake



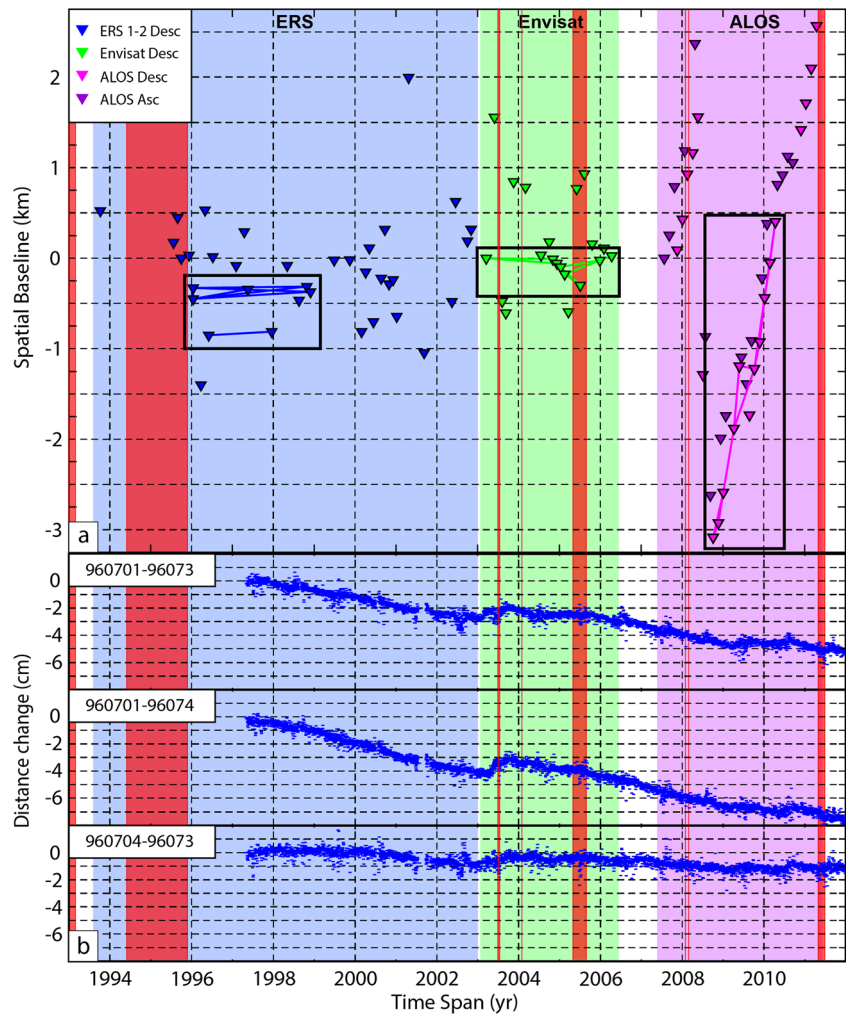
radar (SAR) images from 1993 to 2011 (Fig. 2a) to produce interferograms to evaluate ground displacements. The time span includes most of the recent eruptions (Table 1). This approach allows us to constrain the occurrence of these repeated eruptions in the framework of the longer-term subsidence, as well as the possible cause(s) of subsidence.

## Geologic setting

Aso lies along the western continuation of the Median Tectonic Line (MTL) in central Kyushu Island (Fig. 1). The MTL accommodates part of the dextral component of the relative convergence between the Philippine Sea plate and the Eurasian plate (Aoki and Scholz 2003); in central Kyushu, the MTL carries an extensional component, forming the N-S Beppu-Shimabara graben (Kamata and Kodama 1999; Takayama and Yoshida 2007) that hosts the caldera. Aso caldera is 18 by 25 km wide and N-S elongated. It was formed by four major explosive eruptions between 270 and 90 ka with a total volume of  $>200 \text{ km}^3$ . The post-caldera activity consists of at least 17 basaltic to rhyolitic cones and domes emplaced in the central caldera. Nakadake is the only current active vent, erupting basalts to andesites (Miyabuchi and Sugiyama 2011; Miyoshi et al. 2012). We summarized the recent unrest and eruptive events at Nakadake in Table 1. Nakadake had

phreatomagmatic eruptions from 1989 to 1991, followed by mud eruptions in 1992, 1994 and 1995, all with Volcanic Explosivity Index (VEI) = 2. From 1995 to 2008, a crater lake formed and the temperature increased from 28 to 82 °C. Episodic phreatomagmatic activity and ash fall took place at the Nakadake crater lake from 2003 to 2005 in response to newly ascending magma (Ikebe et al. 2008; Miyabuchi et al. 2008; Siebert et al. 2010). Longer-term levelling surveys of the caldera from 1937 to 2004 show an overall subsidence of  $\sim 7$  cm centred at Kusasenri (3 km west of Nakadake; Fig. 1), interrupted by an uplift of 4 cm during 1950s. Then, from 1993 to 2004, the surface of the caldera contracted, with a subsidence of 1.5 cm (Sudo et al. 2006). GPS data highlight a brief phase of extension in 2003, likely associated with minor uplift (Fig. 2b; Ohkura and Oikawa 2008; Geospatial Information Authority of Japan 2011; Unglert et al. 2011). This, together with gas measurements and low frequency seismic swarms focused in a deep low velocity layer, suggests that a small volume of magma intruded as a sill at  $\sim 15$  km depth and triggered the 2003–2005 phreatomagmatic activity, characterized by 8–9% of juvenile material (Miyabuchi et al. 2008; Abe et al. 2010; Unglert et al. 2011). A deeper low-velocity layer, containing at most 15% melt or 30% aqueous fluid, has been detected between 10 and 24 km beneath the western part of the caldera (Abe et al. 2010). Tomographic data highlight a low-velocity zone, possibly a shallow magma reservoir, at 5–

**Fig. 2 a** Spatial and temporal distribution of SAR images for Aso acquired between 1993–2012 and used in this study. *Triangles* are the image acquisitions, in *blue* are the ERS 1–2 images (Track 475; by Supersite project – Unavco), in *green* are the ENVISAT images (track 475; ESA CAT 1; Acocella responsible) and descending (track 73) and ascending (track 423) ALOS images are respectively in *magenta* and *violet* (PIXEL—PALSAR Interferometry Consortium to Study our Evolving Land surface). *Rectangles* highlight periods with interferograms (*solid lines*) used to evaluate mean deformation rate maps. **b** GPS relative baseline time series (April 1997–December 2012) between three stations installed inside Aso caldera (Geospatial Information Authority—<http://www.gsi.go.jp>). For both images, *red areas* are eruptive periods associated with both phreatic or phreatomagmatic activity of Nakadake (Table 1). *Blue, green* and *violet* areas are periods covered by ERS, Envisat and ALOS SAR images



6 km depth below Kusasenri (Fig. 1; Sudo and Kong 2001; Sudo et al. 2006). The caldera continued to subside until 2011. More

recently, Strombolian activity started at Aso on 25 November 2014 and continued with intermittent activity until the end of

**Table 1** Recent unrest and eruptive events at Nakadake crater (Japan Meteorological Agency 2013; Global Volcanism Program 2016)

Start date	End date	VEI	Type	Eruptive vent
1989 Apr 5	1991 Feb 9	2	Phreatomagmatic eruptions	Nakadake
1992 Apr 23	1993 Jun (?)	2	Mud eruptions	Nakadake
1994 May 2	1995 Nov (?)	2	Mud eruptions	Nakadake
1997	2002		Hot crater lake	Nakadake
2003 Jul 10	2003 Jul 14	1	Ash fall	Nakadake
2004 Jan 14	2004 Jan 14	1	Ash fall	Nakadake
2005 Apr 14	2005 Aug (?)	1	Phreatomagmatic eruptions	Nakadake
2008 Feb 17	2008 Feb 17	1	Phreatomagmatic eruption	Nakadake
2009 Feb 4	2009 Feb 4	1	Tephra fall	Nakadake
2009 Nov 2	2010 Jul		Seismic swarm	
2011 May 15	2011 Jun 9	1	Tephra fall	Nakadake
2014 Jan 13	2014 Feb 19	1	Phreatomagmatic eruption	Nakadake
2014 Aug 30	2015 May 1	2	Strombolian eruption	Nakadake
2015 Sep 3	2015 Oct 23	2	Phreatomagmatic eruption	Nakadake
2016 Mar 4	2016 Apr 16	1	Ash falls	Nakadake

May 2015 (Global Volcanism Program 2015; Japan Meteorological Agency 2015). The eruption was preceded by increased  $\text{SO}_2$  emission of up to 3000 t/day and increased magnitude of volcanic tremors. The total volume of ejecta (almost completely juvenile) is  $\sim 0.8 \times 10^{-3} \text{ km}^3$  Dense Rock Equivalent (DRE; Yasuo Miyabuchi, personal communication). No clear ground deformation associated with the eruption has been observed.

On 15 April 2016, an earthquake swarm, with maximum  $M_w = 7.1$ , hit Kumamoto city, resulting from transtensive dextral faulting at shallow depth (10 km—Lin et al. 2016; Ozawa et al. 2016); surface ruptures reached inside the caldera where a small ash puff originated at Nakadake crater (Japan Meteorological Agency 2016; Global Volcanism Program 2016; Miyakawa et al. 2016).

## Methodology

### InSAR processing

We processed 97 SAR images from October 1993 to April 2011 (Fig. 2a); these include 34 images from the European Remote Sensing (ERS) 1–2 satellites (October 1993–November 2002), 20 images from the Environmental Satellite (ENVISAT—February 2003–March 2006) and 43 images from the Advanced Land Observing Satellite (ALOS—January 2007–April 2011). For each satellite, we selected image pairs to form >220 interferograms with

perpendicular baselines <500 m (1000 m for ALOS) and a time span between acquisitions of <3 year. Data have been processed using the Repeat Orbit Interferometry Package (ROI\_PAC—Rosen et al. 2004). The topographic phase is removed using the 3-arc-second Shuttle Radar Topography Mission Digital Elevation Model (SRTM DEM—Farr et al. 2007). Interferograms were unwrapped using a branch-cut algorithm (Goldstein et al. 1988). Because of the partly steep topography, vegetation and, at times, snow coverage, shorter wavelength (C-band  $\sim 6$  cm) ERS and ENVISAT interferograms with spatial baseline >200 m were incoherent, in contrast to the longer wavelength (L-band  $\sim 24$  cm) ALOS interferograms. In addition, most of the interferograms had a low signal-to-noise ratio and weak displacement signal.

Analysing single interferograms, we were able to identify a consistent and homogeneous subsidence signal (<1 cm/year) in the central part of the caldera. To increase the signal-to-noise ratio and reduce the non-deformation phase contribution, we post-processed unwrapped interferograms, in periods covered by several images (Fig. 2a), with Poly-Interferogram Rate And Time-series Estimator (Pi-RATE) software to produce mean deformation rate maps (Wang et al. 2009, 2012). This software uses redundant interferograms to highlight and discard pixels affected by unwrapping errors with the phase closure technique (Biggs et al. 2007). With the minimum spanning tree algorithm (Kruskal 1956), Pi-RATE selects the non-redundant observations according to the unwrapped fraction of the interferograms. Pi-RATE uses all the coherent pixels in the non-redundant interferograms, and when

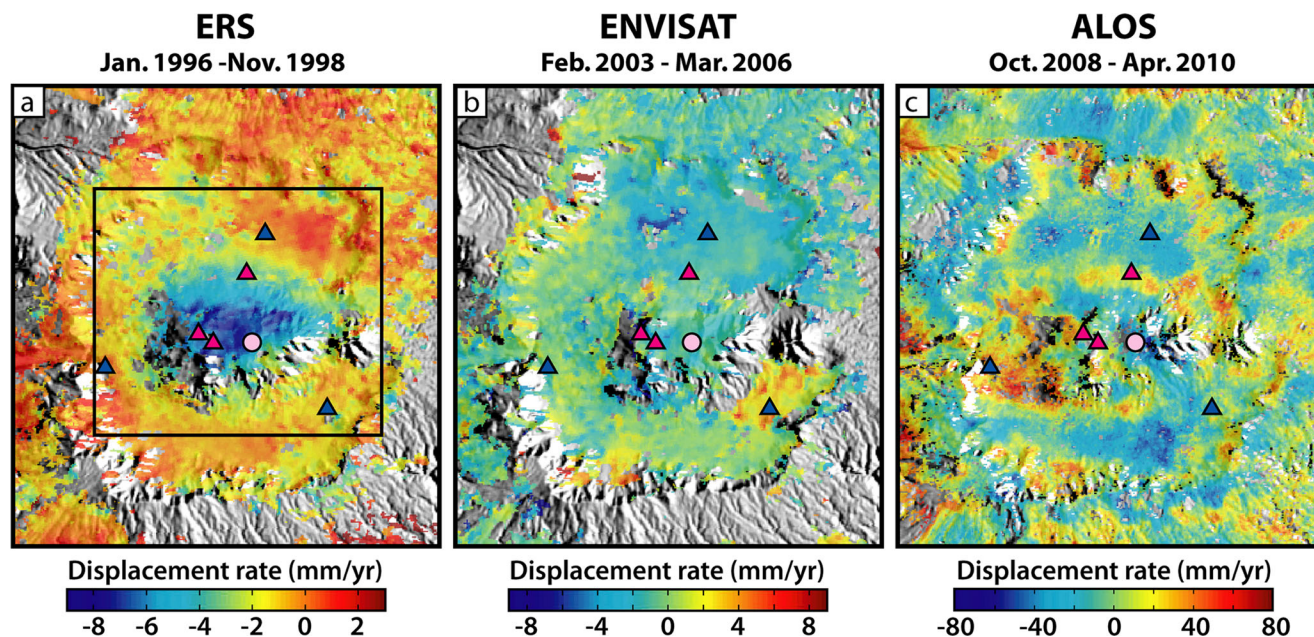


**Fig. 3** a, b, c The InSAR mean deformation rate maps evaluated with Pi-RATE software for ERS, ENVISAT and ALOS data respectively. *Blue triangles* are GPS stations (Geospatial Information Authority of Japan

2011) and *magenta triangles* are levelling benchmarks (Sudo et al. 2006). *Pink circle* is the Nakadake crater. The *rectangle* in a corresponds to the area modelled (Fig. 4)

possible, it recovers the non-coherent pixels from the corresponding data in the redundant interferograms. It estimates residual orbital phase ramps using quadratic polynomial models and stratified tropospheric phase contributions using a linear function of the DEM based on a network approach (Biggs et al. 2007; Elliott et al. 2008) for each interferogram. It then estimates a temporal-spatial filter using a raw deformation time series, assuming that the signal is temporally random and spatially correlated (Ferretti et al. 2001). Finally, it stacks non-redundant and corrected pixels to evaluate the mean rate deformation map. Pi-Rate software evaluates also the measurements error for the deformation rate. This is the mathematical evaluation of the error on the phase difference measurements. It does not account for the non-deformation phase contribution that it is not removed during the interferograms post-processing and can locally reach high values (few cm/year depending on the sensor).

We produced three mean rate deformation maps (Fig. 3) using interferograms from different sensors: 8 ERS interferograms (3 redundant) cover the January 1996–November 1998 period (Table 2); 11 Envisat interferograms (4 redundant), with minor unwrapping errors, form a chain from February 2003 to March 2006 (Table 2). Although ALOS interferograms were coherent, we observed a strong correlation between atmospheric phase contribution and topography so we used only 13 interferograms (4 redundant) between October 2008 and April 2011 (Table 2) with a small baseline (<650 m), to minimize the topographic effect.

### Analytical model inversion

The ERS displacement rate map shows a higher signal-to-noise ratio and a clearer deformation pattern within the caldera compared to the Envisat and ALOS data. Therefore, we inverted the deformation rate map and tested three different deformation sources, including a deflating point source (Mogi 1958); a sill-like source modelled as a horizontal plane closure (Okada 1985) and a deflating ellipsoid (Yang et al. 1988) buried in an homogeneous, elastic half-space with flat topography and a Poisson's ratio = 0.25. Before the inversion, the number of data points was subsampled using a quadtree algorithm (Jónsson et al. 2002), reducing the data points from >33,500 to 2520. To obtain the best-fit model, we used a non-linear inversion consisting of a simulated annealing (SA) optimization technique (Cervelli et al. 2001) that minimizes residuals. Uncertainties about parameters for this best-fit model were calculated using a Monte-Carlo simulation in which correlated noise was added to the data to obtain 250 noisy samples of the observations; these 250 noisy models were then inverted again using the SA technique, obtaining 250 new sets of model parameters used to estimate the confidence interval (Figs. SM1 to SM3; Wright et al. 2003).

Since our dataset shows a low signal-to-noise ratio, when the Monte Carlo synthetic noise is added to the

signal to evaluate the confidence interval for the model parameters, the observed displacement may change in both position and amplitude. When the signal plus the noise are inverted using the SA technique, the evaluated parameters are different from the best model obtained inverting only the signal. This can result in a larger confidence interval and non-Gaussian distribution of the histograms for some parameters of the inversions.

**Table 2** Interferograms used to create mean deformation rate maps

Pairs	Spatial BL (m)	Temp BL (year)
ERS track 475		
19960113_19960114	−121	0.00
19960113_19970518	−22	1.35
19960113_19981025	17	2.78
19960113_19981129	−55	2.88
19960114_19970518	99	1.34
19960114_19981025	137	2.78
19960114_19981129	66	2.87
19960601_19971214	33	1.54
Envisat track 475		
20030216_20041003	−10	1.63
20030216_20041107	−57	1.73
20041003_20041107	−46	0.09
20041107_20041212	−40	0.10
20041107_20050116	−120	0.19
20041212_20050116	−80	0.09
20041212_20050605	−203	0.48
20041212_20051127	74	0.96
20050116_20050605	−124	0.39
20050116_20051127	153	0.86
20051127_20060312	50	0.29
ALOS track 73		
20081012_20081127	156	0.12
20081012_20090112	485	0.25
20081127_20090112	329	0.13
20090112_20090414	696	0.26
20090414_20090530	688	0.13
20090414_20091015	650	0.50
20090530_20091015	−38	0.38
20091015_20091130	293	0.12
20091015_20100115	777	0.25
20091130_20100115	485	0.13
20100115_20100302	382	0.13
20100115_20100417	829	0.26
20100302_20100417	447	0.12

BL baseline



**Table 3** Source parameters obtained by the inversion of levelling data (Sudo et al. 2006) and InSAR data

	Lat.	Lon.	Depth (km)	$\Delta V$ ( $10^{-3}$ km <sup>3</sup> /year)	Op. (cm/year) $\Delta P$ (MPa/year)	Data variance
Levelling	32.86	131.05	5.8	-0.9	-	-
Mogi	32.89	131.07	4.1	-0.6	-	33.3%
Sill	32.89	131.07	5.1	-0.6	-1.8	33.3%
Ellipsoid	32.88	131.07	4.7	-0.3	-30.7	33.3%

## Results

### InSAR and Modelling

Continuous subsidence of the central caldera between January 1996 and November 1998 is highlighted by ERS data (Fig. 4a). The displacement rate map shows pronounced E-W elongated subsidence with a maximum displacement of 9 mm/year in the satellite line of sight (LOS) within the caldera, centred slightly (1.5 km) to the north of the post-caldera vents. We used analytical models to evaluate the source parameters for this subsidence (Fig. 4). Model parameters, including the depth (in km), the volumetric variation (in  $10^{-3}$  km<sup>3</sup>/year), the opening (cm/year) or pressure variation

(in MPa) and the data variance for each source are reported in Table 3.

The Mogi source is the shallowest that we obtained (4.1 km deep) and lies slightly NE of Nakadake (Fig. 4b). The sill-like source is the deepest (5.2 km deep) and is E-W elongated (Fig. 4c). Looking at the profile of the deformation (Fig. 4), the sill-like source seems a better fit to the E-W elongated pattern of the subsidence. The volume change of the sill source is very similar to that of the Mogi source ( $\sim 0.6 \times 10^{-3}$  km<sup>3</sup>); however, the observed maximum displacement rate is lower ( $\sim 1$  mm/year). The ellipsoid source lies roughly below Nakadake (Fig. 4d) and its depth (4.7 km) is between the two other sources, the volumetric variation being the smallest ( $\sim 0.3 \times 10^{-3}$  km<sup>3</sup>). The root mean square (RMS) of the residual between observation and model is similar for the three sources (1.4 mm/year). Residuals between the observed subsidence and the models are generally very small (Fig. 4d–f) with the exception of the upper right corner of the rate map (Fig. 4a), which has a higher residual. We report model parameter uncertainties with the histograms for the distribution and the correlation graph in Figures SM1 (Mogi source), SM2 (sill) and SM3 (ellipsoid).

Sources with different geometries may show similar deformation patterns (e.g. Dieterich and Decker 1975), especially using a single LOS displacement rate map. For this reason, it is difficult to choose a most-reliable model. RMS residuals for the three sources are also similar and thus not useful for discriminating. If we consider other available geophysical data, the three evaluated sources are located in an aseismic area (Fig. 5) roughly below Nakadake; in particular, they lie in a zone interpreted as a high temperature body, without seismic reflectors (Tsutsui and Sudo 2004).

The deformation rate map for ENVISAT data (February 2003–March 2006) shows weak subsidence (<5 mm) in the central caldera and an uplift area in the ESE, near the 960704 GPS station (Fig. 3b). However, this deformation has not been inverted because the signal was too weak. Similarly, the noisy deformation rate map for the ALOS data (October 2008–April 2010; Fig. 3c) has not been inverted. ALOS interferograms are coherent due to the longer wavelength; they are less sensitive to small ground deformations and contain a major contribution of atmospheric delay.

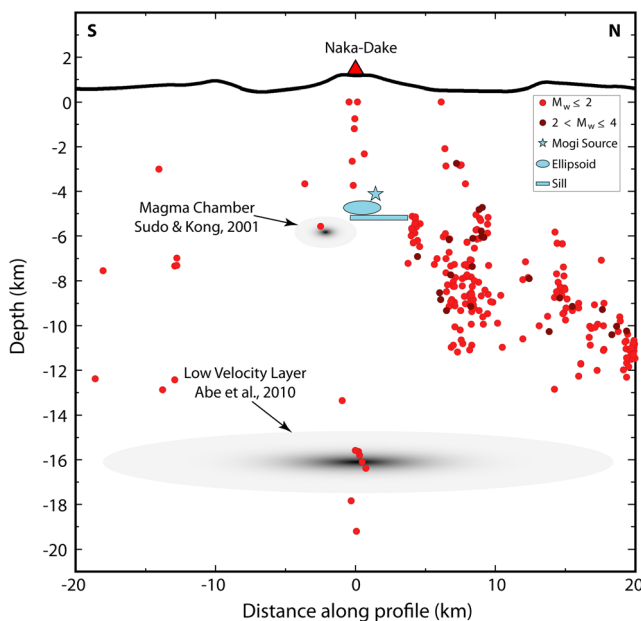


**Fig. 5** N-S upper crustal section beneath Aso caldera. Red circles = earthquakes detected between January 1990–September 2011 (Earthquakes Research Institute, Japan). Grey areas indicate the shallower low-velocity zone interpreted as a magma chamber (Sudo and Kong 2001), corresponding to the levelling deformation source of Sudo et al. (2006) and the central part of the deeper low-velocity layer observed with the receiver functions by Abe et al. (2010). Cyan star is the Mogi source; cyan horizontal line is the sill; cyan ellipse is the projection of the ellipsoid obtained in this study

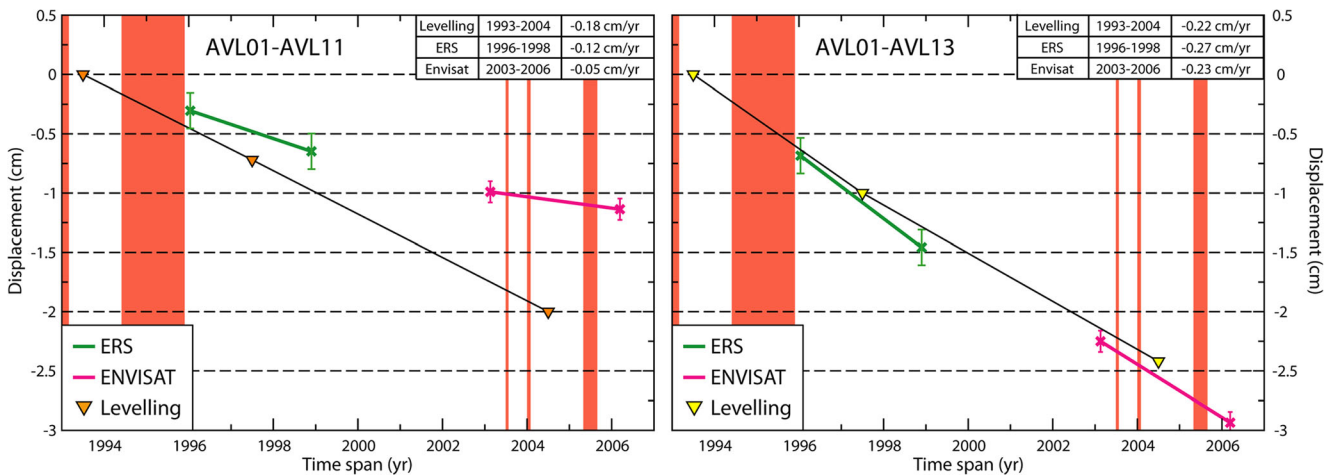


**Fig. 6** Relative displacement for benchmarks AVL11 and AVL13 with respect to AVL01 (location in Fig. 1) evaluated using levelling data (Sudo et al. 2006) compared with InSAR displacement rates for ERS and ENVISAT data. ERS and Envisat measurements errors ( $\pm 1.5$  and

$\pm 0.9$  mm/year respectively) estimated by Pi-Rate are included. The inset tables report the respective relative mean deformation rate (cm/year) obtained from the three levelling points (1993–1997–2004) and the InSAR data

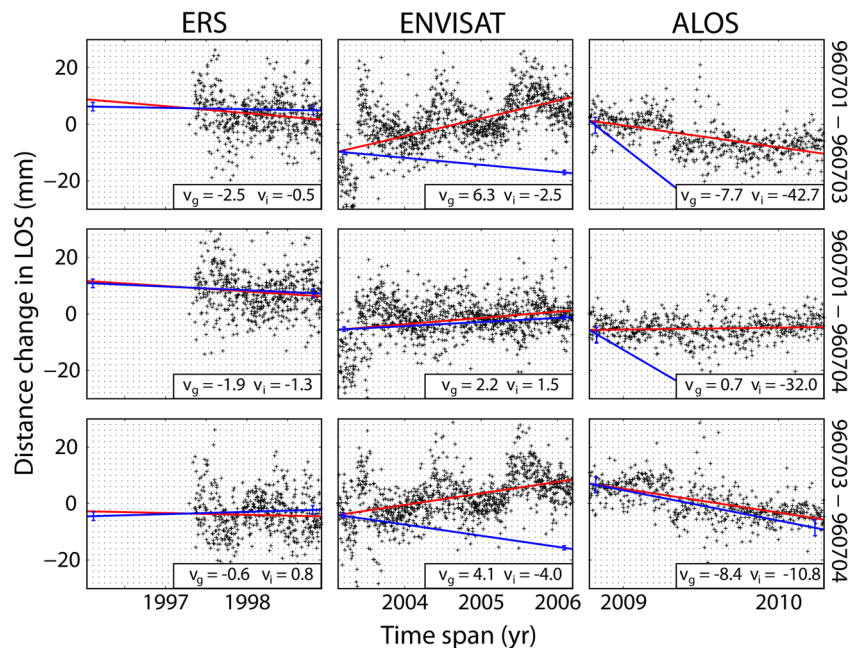
Indeed, we observed a strong correlation between atmospheric phase contribution and topography on single ALOS interferograms. Although we use interferograms with shorter spatial baselines (<650 m; Table 2) to minimize the topographic effect, the mean deformation rate map obtained from Pi-RATE retains a high signal-to-topography correlation.

**Comparison with levelling and GPS data**

To better determine the deformation rate, the InSAR data are compared with the available levelling and GPS data for the

central part of the caldera (Figs. 6 and 7: Sudo et al. 2006; Geospatial Information Authority 2011—<http://www.gsi.gov.jp>). Levelling data between 1993 and 2004 (three acquisitions) were collected at benchmarks AVL11 (Kusanseri crater) and AVL13 (near Nakadake crater); the displacements are referenced to AVL01, which is considered stable (Sudo et al. 2006). We extracted the InSAR deformation rate for pixels within 250 m of the levelling benchmarks, reporting the relative velocities in Fig. 6. Here, ERS data are in general in agreement with the levelling observations. The comparison between ENVISAT and levelling deformation

**Fig. 7** Comparison between GPS and InSAR baseline variation. *Black plus signs* are the GPS baselines rotated in LOS. The *red lines* are the GPS mean velocity obtained by a linear fit from the GPS time series. The *blue lines* are the mean relative InSAR velocities for all the pixels within 250 m from the GPS station. We included the ERS, Envisat and ALOS deformation rate errors estimated by Pi-Rate ( $\pm 1.5$ ,  $\pm 0.9$  and  $\pm 2.8$  mm/year respectively). The respective distance change velocities for GPS ( $v_g$ ) and InSAR ( $v_i$ ) are reported in each graph



rates suggests that the subsidence in the central part of the caldera continued until 2006, even though AVL11 shows a slower subsidence rate. As for the GPS data, three GPS stations have been installed inside the caldera since April 1997 (Ohkura and Oikawa 2008; Geospatial Information Authority of Japan 2011). Stations lie in the plain below the post-caldera vents (Figs. 1 and 3), far from the area that shows maximum displacement. In general, the stations show shortening of 1–5 mm/year on the relative baseline (Fig. 2b), which is interpreted as subsidence of the central part of the caldera. An exception occurred between May and November 2003, when the baselines increased by ~5 mm; this is interpreted as uplift associated with a sill intruded at ~15 km depth (Ohkura and Oikawa 2008; Unglert et al. 2011). Here, we take into account GPS data from the three periods covered by InSAR deformation rate maps. We then rotate the observed GPS baselines in the respective satellite LOS and evaluate the mean distance variation with a linear fit ( $v_g$ ). We then extract the InSAR deformation rate for pixels within 250 m of the GPS stations and evaluate the relative mean displacement velocity ( $v_i$ ; Fig. 7). For the period covered by ERS data, the Baseline Variation Velocity (BVV) is similar for the GPS and InSAR measurements, and for all stations, it ranges between 0 and 2.5 mm/year. Considering the Envisat data, the BVV is similar between stations 960701 and 960704 measured with the two techniques (~2 mm/year). The relative velocity of 960701 and 960704 with regard to 960703 shows a different behaviour. The GPS velocity is positive and increases (4–6 mm/year); the InSAR velocity is negative and decreases from –2 to –4 mm/year. The ALOS BVV between stations 960703 and 960704 is in broad agreement with GPS data ( $v_g = 8$  mm/year and  $v_i = 11$  mm/year). However, a major difference is observed for the BVV of 960703 and 960704 with regard to 960701, where the  $v_g$  varies between 1 and –7 mm/year and  $v_i$  between –32 and 42 mm/year. The difference between the GPS and InSAR velocities may be due to local noise that affects particularly Envisat and ALOS deformation rate maps. This is clear for ALOS data where (Fig. 3c) the westernmost GPS station (960701) is located in a noisy area, where the signal is +30 mm/year. Instead, the difference in the ENVISAT data for the northernmost GPS station (960703) could be due to the GPS measuring correctly the movement along the NS direction, which cannot be detected by InSAR. This comparison confirms that, in our analysis, the ERS data are more reliable than that from the other sensors.

## Discussion

### Evidence for magma-related deformation

The Pi-RATE software enhances smoothing of the interferometric signal by discarding the noisiest interferograms,

correcting for imperfect orbital knowledge, atmospheric propagation delays and topographic errors before stacking the interferograms. As also shown in Figs. 6 and 7, the displacement rate obtained with Pi-RATE for the ERS data agrees with the levelling and GPS deformation field. Even though inversion of the InSAR data from a single track may not allow an optimal constraint of the spatial parameters of the source, the modelled sources for the ERS displacement rate map are all located below the active Nakadake crater. The depth of the modelled sources ranges between 4 and 5 km below the surface and is consistent with all the available seismic and gas emission data (Ono et al. 1995; Sudo and Kong 2001; Tsutsui and Sudo 2004; Abe et al. 2010; Unglert et al. 2011): this depth suggests a magmatic deformation source, making any significant contribution from a shallower hydrothermal system unlikely. The models account for the subsidence in the central part of the caldera, while the residuals are mainly associated with noise in peripheral areas. The weak deformation signal is only slightly larger than the noise, so the noise contribution to the residual RMS is substantial. The overall locations of our sources are broadly consistent with those from previous studies, although with a slight shift (~2 km to the north and 1 km to the east—Fig. 5; Sudo and Kong 2001; Sudo et al. 2006; Unglert et al. 2011). All sources lie above a low velocity layer located at ~16 km depth (Abe et al. 2010), identified also as the source of long period tremors (Kawakatsu et al. 2000), which may coincide with a deeper magmatic reservoir feeding the shallower one (Fig. 5).

The 1996–1998 period of subsidence marks an important point in the recent evolution of Aso, as it follows a long period of volcanic activity with the 1989–1991 period of phreatomagmatic eruptions and the mud eruptions in 1992–1993, 1994 and 1995. Since then, the crater has filled with an acid water lake. It is challenging to clearly establish whether our investigated period reflects temporal variation in the previously detected long-term deflation rate (Sudo et al. 2006) or if it is simply the result of a different time sampling of the available SAR images. Also, the subsidence rates deduced from the levelling, based on only four measurements in 23 years (from 1981 to 2004; Sudo et al. 2006), may not be representative of a linear behaviour and may rather be characterized by larger, undetected variations, as for example shown by GPS data in 2003 (Fig. 2b). However, as the calculated InSAR (ERS) subsidence rates are in general similar to the ones obtained from levelling (Fig. 6) and GPS (Fig. 7), it is probable that the detected InSAR deformation is only a portion of a larger, continuous and fairly constant subsidence. In this sense, our study confirms the subsidence detected through levelling and GPS data and suggests that the 1996–1998 period is representative of the behaviour of the volcano over the last decades. Below, we use this information to better constrain the magmatic sources responsible for the deformation and the associated processes.

## The importance of outgassing

Aso is intriguingly the only monitored caldera experiencing long-term deflation while characterized at the same time by phreatomagmatic eruptions, even though minor (VEI = 2). Our results suggest that the deflation at Aso may reflect pressure variations in a magmatic source located at 4 and 5 km depth, rather than to pressure fluctuations of shallow fluids in a hydrothermal system. Several calderas have been experiencing long-term deflation without any eruption, as at Askja and Krafla, Iceland (e.g. Sturkell and Sigmundsson 2000; Pagli et al. 2006; Sturkell et al. 2008). While at Askja the subsidence is probably caused by a cooling and contracting magma chamber (De Zeeuw-van Dalssen et al. 2013); at Krafla, the post-1984 gravity decrease suggests that the subsidence is related to drainage from a shallow magma chamber (Rymer et al. 1998). At both calderas, a shallow magma chamber seems to have played an important role in the subsidence.

Despite the differences in magma composition and tectonic setting of Askja and Krafla, deflation at Aso may have been induced by a similar process of contraction of a shallow magma chamber. However, in contrast to Krafla and Askja, the repeated minor eruptions at Aso suggest that the contraction may not be necessarily related to cooling. Rather, the contraction may be induced by a significant release of magmatic fluids (mostly CO<sub>2</sub>, SO<sub>2</sub> and H<sub>2</sub>O) from the magma reservoir to the hydrothermal system and of juvenile magma, enhanced by the diffuse outgassing. Both the fluids and the magma may be periodically released through the observed phreatomagmatic eruptions. A similar mechanism has been suggested for several volcanoes (e.g. Satsuma-Iwojima and Asama, in Japan; Masaya in Nicaragua and Llaima, in Chile), where outgassing-induced depressurization may have accounted for the subsidence observed during quiescence (Girona et al. 2014, and references therein).

Unfortunately, in the case of Aso, we do not have access to any continuous SO<sub>2</sub> and CO<sub>2</sub> emission rate to better constrain the outgassing process. However, the possibility of an important role played by outgassing is partly supported by available estimates at the erupted volumes at Aso in the last decades:  $5 \times 10^{-3}$  km<sup>3</sup> (DRE) in the 1989–1991 eruption (Ono et al. 1995) and  $0.8 \times 10^{-3}$  km<sup>3</sup> (DRE) in the 2014–2015 eruption (Yasuo Miyabuchi, personal communication). Even though measurements are not available, each phreatomagmatic eruption from 1991 to 2014 is expected to have erupted no more than  $0.2 \times 10^{-3}$  km<sup>3</sup> (DRE; Miyabuchi et al. 2008). These estimates are similar to our inferred volumetric variations in the magma reservoir, estimated to be between  $0.25 \times 10^{-3}$  and  $0.57 \times 10^{-3}$  km<sup>3</sup>/year (depending on the source type). All these features suggest a possible correlation between eruptive outgassing via hydrothermal eruptions at the surface and contraction of the source. Because of the uncertainties in both the outgassing and contraction estimates, especially taking into account fluid compressibility, we consider this relation as a working hypothesis, to be further tested by future studies. If this

correlation were to be confirmed, it could imply (1) a lack of shallow magmatic intrusions, suggesting that magma emplaced into the volcano is currently restricted to the main magmatic source described in this study and (2) that outgassing may aid in transferring some limited amount of magma toward the surface, promoting minor phreatomagmatic eruptions.

More generally, many calderas are characterized by continuous outgassing, similarly to Aso; these include Iwo-Jima, Yellowstone and Campi Flegrei. These outgassing systems, continuously releasing their energy through magmatic fluids, may prevent the pressure build-up required to trigger moderate to large eruptions (Acocella et al. 2015). Aso lies on the upper bound of these calderas, as it shows that magmatic outgassing may be accompanied by minor phreatomagmatic eruptions. Even more important, processes at Aso are associated with deflation, unlike the other calderas which commonly show inflation. This raises a more general and crucial point, which is that eruptions may occur in a context of overall subsidence of a volcanic edifice. While surface inflation may not necessarily be diagnostic for forecasting an impending eruption, at least at calderas (Acocella et al. 2015, and references therein), the possibility that a deflating caldera can erupt remains worrisome; our current understanding of magmatic models foresees eruptions resulting from an increase of pressure within the magma reservoir, thus leading to volcano inflation. Conversely, the example of Aso suggests that outgassing processes may play a crucial role in triggering minor non-magmatic eruptions within open conduit calderas, as also suggested for other volcanoes (Girona et al. 2014): indeed, if our hypothesis is correct, the crucial ingredient to cause eruptions from deflating calderas is substantial outgassing and an open magmatic conduit. Both features distinguish the repeated outgassing episodes at Aso, culminating in minor hydrothermal eruptions, from the non-eruptive unrest episodes at other active felsic calderas, as for example Campi Flegrei. At Campi Flegrei, despite the detection of repeated outgassing episodes (Chiodini et al. 2012, 2015, 2016), the lack of an open magmatic conduit may currently hinder eruptive activity driven by outgassing alone. In this way, outgassing may allow energy release from the system through hydrothermal activity, uplift and seismicity (e.g. Chiodini et al. 2003).

Our study thus underlines the importance of considering and trying to better define the eruptive potential from deflating magmatic systems with open magmatic conduits, where the energy may be released at different times through hydrothermal activity, seismicity and inflation.

## Conclusions

We used InSAR data to investigate surface deformation at the repeatedly erupting Aso caldera, Japan. Despite an overall low signal-to-noise ratio, we observe a subsidence signal from 1996 to 1998, inferred to be associated with overall

contraction of a magmatic source below the caldera centre, at 4 to 5 km depth. Available data suggest that the volume of source contraction is similar to that of erupted material. We thus propose that the contraction may have been induced by the release of magmatic fluids, transferring a minor amount of magma toward the surface and driving phreatomagmatic eruptions. If confirmed by further observations, this hypothesis suggests that outgassing processes may play a crucial role in triggering minor phreatomagmatic eruptions within open conduit calderas, such as at Aso. Based on our study, we propose that the crucial ingredients for deflating calderas to erupt include substantial outgassing and an open magmatic conduit. Under these conditions, the energy may be released at different times and places by the hydrothermal activity, seismicity and inflation that commonly characterize unrest.

**Acknowledgments** This study was made in the framework of an ESA Category 1 proposal 7486 (V. Acocella responsible). The Supersite initiative (F. Amelung and S. Gross) is gratefully acknowledged for providing Envisat images. PALSAR level 1.0 data from the ALOS satellite are shared among PIXEL (PALSAR Interferometry Consortium to Study our Evolving Land surface) and provided by the Japan Aerospace Exploration Agency (JAXA) under a cooperative research contract with the Earthquake Research Institute, University of Tokyo. The ownership of PALSAR data belongs to the Ministry of Economy, Trade and Industry, and JAXA. G. Chiodini, E. Sansosti and M. Poland provided useful suggestions on an earlier version of the manuscript. We also would like to thank F. Costa and an anonymous reviewer who provided detailed reviews to improve the manuscript. Finally, thanks to the Associated Editor K.V. Cashman and to the Executive Editor J.D.L. White for additional comments that enhanced this work.

## References

- Abe Y, Ohkura T, Shibutani T, Hirahara K, Kato M (2010) Crustal structure beneath Aso caldera, Southwest Japan, as derived from receiver function analysis. *J Volcanol Geotherm Res* 195(1):1–12. doi:10.1016/j.jvolgeores.2010.05.011
- Acocella V, Di Lorenzo R, Newhall C, Scandone R (2015) An overview of recent (1988 to 2014) caldera unrest: knowledge and perspectives. *Rev Geophys* 53. doi:10.1002/2015RG000492
- Aoki Y, Scholz CH (2003) Interseismic deformation at the Nankai subduction zone and the Median tectonic line, Southwest Japan. *J Geophys Res* 108(B10):2470. doi:10.1029/2003JB002441
- Biggs J, Wright TJ, Lu Z, Parsons B (2007) Multi-interferogram method for measuring interseismic deformation: Denali fault, Alaska. *Geophys J Int* 170:1165–1179. doi:10.1111/j.1365-246X.2007.03415.x
- Cervelli P, Murray M, Segall P, Aoki Y, Kato T (2001) Estimating source parameters from deformation data, with an application to the March 1997 earthquake swarm off the Izu peninsula, Japan. *J Geophys Res* 106:11,217–11,238
- Chiodini G, Todesco M, Caliro S, Del Gaudio C, Macedonio G, Russo M (2003) Magma degassing as a trigger of bradyseismic events: the case of Phlegrean fields (Italy). *Geophys Res Lett* 30:1434. doi:10.1029/2002GL016790
- Chiodini G, Caliro S, De Martino P, Avino R, Gherardi F (2012) Early signals of new volcanic unrest at Campi Flegrei caldera? Insights from geochemical data and physical simulations. *Geology* 40(10):943–946. doi:10.1130/G33251.1
- Chiodini G, Vandemeulebrouck J, Caliro S, D’Auria L, De Martino P, Mangiacapra A, Petrillo Z (2015) Evidence of thermal-driven processes triggering the 2005–2014 unrest at Campi Flegrei caldera. *Earth Planet Sci Lett* 414:58–67. doi:10.1016/j.epsl.2015.01.012
- Chiodini G, Paonita A, Aiuppa A, Costa A, Caliro S, De Martino P, Acocella V, Vandemeulebrouck J (2016) Hotter volcanic unrest for magmas near the critical degassing pressure. *Nat Commun*. doi:10.1038/ncomms13712
- de Zeeuw-van Dalzen E, Rymer H, Sturkell E, Pedersen R, Hooper A, Sigmundsson F, Ófeigsson B (2013) Geodetic data shed light on ongoing caldera subsidence at Askja, Iceland. *Bull Volcanol* 75(5):709. doi:10.1007/s00445-013-0709-2
- Dieterich JH, Decker RW (1975) Finite element modeling of surface deformation associated with volcanism. *J Geophys Res* 80(29):4094–4102
- Elliott JR, Biggs J, Parsons B, Wright TJ (2008) InSAR slip rate determination on the Altyn Tagh fault, northern Tibet, in the presence of topographically correlated atmospheric delays. *Geophys Res Lett* 35:L2309. doi:10.1029/2008GL033659
- Farr TG, Rosen PA, Caro E, Crippen R, Duren R, Hensley S, Kobrick M, Paller M, Rodriguez E, Roth L, Seal D, Shaffer S, Shimada J, Umland J, Werner M, Oskin M, Burbank D, Alsdorf D (2007) The shuttle radar topography mission. *Rev Geophys* 45(2). doi:10.1029/2005RG000183
- Ferretti A, Prati C, Rocca F (2001) Permanent scatterers in SAR interferometry. *IEEE Trans Geosci Remote* 39(1):8–20
- Geospatial Information Authority of Japan (2011) Crustal deformations around Aso volcano. [http://www.data.jma.go.jp/svd/vois/data/tokyo/STOCK/kaisetsu/CCPVE/Report/107/kaiho\\_107\\_24.pdf](http://www.data.jma.go.jp/svd/vois/data/tokyo/STOCK/kaisetsu/CCPVE/Report/107/kaiho_107_24.pdf) (in Japanese)
- Girona T, Costa F, Newhall C, Taisne B (2014) On depressurization of volcanic magma reservoirs by passive degassing. *Journal of Geophysical Research: Solid Earth* 119(12):8667–8687. doi:10.1002/2014JB011368
- Global Volcanism Program (2015) Report on Asosan (Japan). In: Wunderman, R (ed.), *Bulletin of the Global Volcanism Network*, 40:2. Smithsonian Institution and US Geological Survey
- Global Volcanism Program (2016) Report on Asosan (Japan). In: Sennert, S K (ed.), *Weekly Volcanic Activity Report*, 20 April–26 April 2016. Smithsonian Institution and US Geological Survey
- Goldstein RM, Zebker HA, Werner CL (1988) Satellite radar interferometry: two-dimensional phase unwrapping. *Radio Sci* 23(4):713–720
- Ikebe S, Watanabe K, Miyabuchi Y (2008) The sequence and style of the 1988–1995 eruptions of Nakadake, Aso volcano, Kyushu. *Japan Bull Volcanol Soc Jap* 53:15–33
- Japan Meteorological Agency (2013) National Catalogue of the Active Volcanoes in Japan (fourth edition, English version). [http://www.data.jma.go.jp/svd/vois/data/tokyo/STOCK/souran\\_eng/volcanoes/084\\_asosan.pdf](http://www.data.jma.go.jp/svd/vois/data/tokyo/STOCK/souran_eng/volcanoes/084_asosan.pdf)
- Japan Meteorological Agency (2015) Monthly report on earthquakes and volcanoes in Japan, December 2015. Pp. 141
- Japan Meteorological Agency 2016 [https://ds.data.jma.go.jp/svd/vaac/data/Archives/2016\\_vaac\\_list.html](https://ds.data.jma.go.jp/svd/vaac/data/Archives/2016_vaac_list.html)
- Jónsson S, Zebker H, Segall P, Amelung F (2002) Fault slip distribution of the 1999 Mw7.1 Hector mine, California, earthquake, estimated from satellite radar and GPS measurements. *Bull Seism Soc Am* 92:1377–1389
- Kamata H, Kodama K (1999) Volcanic history and tectonics of the Southwest Japan arc. *Island Arc* 8:393–403. doi:10.1046/j.1440-1738.1999.00241.x
- Kawakatsu H, Kaneshima S, Matsubayashi H, Ohminato T, Sudo Y, Tsutsui T, Uhira K, Yamasato H, Ito H, Legrand D (2000) Aso94: Aso seismic observation with broadband instruments. *J Volcanol Geotherm Res* 101(1):129–154

- Kruskal JB (1956) On the shortest spanning subtree of a graph and the traveling salesman problem. *Proc Am Math Soc* 7(1):48–50
- Lin A, Satsukawa T, Wang M, Asl ZM, Fueta R, Nakajima F (2016) Coseismic rupturing stopped by Aso volcano during the 2016 Mw 7.1 Kumamoto earthquake, Japan. *Science* 354(6314):869–874. doi: [10.1126/science.aah4629](https://doi.org/10.1126/science.aah4629)
- Miyabuchi Y, Sugiyama S (2011) 90,000-year phytolith record from tephra section at the northeastern rim of Aso caldera, Japan. *Quat Int* 246(1):239–246
- Miyabuchi Y, Ikebe S, Watanabe K (2008) Geological constraints on the 2003–2005 ash emissions from the Nakadake crater lake, Aso volcano Japan. *J of Vol and Geoth Res* 178(2):169–183. doi: [10.1016/j.jvolgeores.2008.06.025](https://doi.org/10.1016/j.jvolgeores.2008.06.025) Volcanic lakes and environmental impacts of volcanic fluids.
- Miyakawa A, Sumita T, Okubo Y, Okuwaki R, Otsubo M, Uesawa S, Yagi Y (2016) Volcanic magma reservoir imaged as a low-density body beneath Aso volcano that terminated the 2016 Kumamoto earthquake rupture. *Earth, Planets and Space* 68(1):208
- Miyoshi M, Sumino H, Miyabuchi Y, Shinmura T, Mori Y, Hasenaka T, Nagao, K (2012) K–Ar ages determined for post-caldera volcanic products from Aso volcano, central Kyushu, Japan. *J Volcanol Geotherm Res* 229:64–73. doi: [10.1016/j.jvolgeores.2012.04.003](https://doi.org/10.1016/j.jvolgeores.2012.04.003)
- Mogi K (1958) Relations between the eruptions of various volcanoes and the deformation of the ground surfaces around them. *Bull Earthq Res Inst U Tokyo* 36:99–134
- Newhall CG, Dzurisin D (1988) Historical unrest at large calderas of the world: USGS Bulletin, v. 1855
- Ohkura T, Oikawa J (2008) GPS observation of crustal movements at Aso volcano. conference paper Fall Meeting, Volcanol. Soc. Jpn., Morioka, Japan (in Japanese)
- Okada Y (1985) Surface deformation due to shear and tensile faults in a half-space. *Bull Seismol Soc Am* 75(4):1135–1154
- Ono K, Watanabe K, Hoshizumi K, Ikebe S (1995) Ash eruption of the Naka-dake crater, Aso volcano, southwestern Japan. *J Volcanol Geotherm Res* 66:137–148. doi: [10.1016/0377-0273\(94\)00061-K](https://doi.org/10.1016/0377-0273(94)00061-K)
- Ozawa T, Fujita E, Ueda H (2016) Crustal deformation associated with the 2016 Kumamoto earthquake and its effect on the magma system of Aso volcano. *Earth, Planets and Space* 68(1):186. doi: [10.1186/s40623-016-0563-5](https://doi.org/10.1186/s40623-016-0563-5)
- Pagli C, Sigmundsson F, Árnadóttir T, Einarsson P, Sturkell E (2006) Deflation of the Askja volcanic system: constraints on the deformation source from combined inversion of satellite radar interferograms and GPS measurements. *J Volcanol Geotherm Res* 152(1–2):97–108. doi: [10.1016/j.jvolgeores.2005.09.014](https://doi.org/10.1016/j.jvolgeores.2005.09.014) ISSN 0377–0273
- Rosen PA, Henley S, Peltzer G, Simons M (2004) Updated repeat orbit interferometry package released. *Eos Trans AGU* 85(5). doi: [10.1029/2004EO050004](https://doi.org/10.1029/2004EO050004).
- Rymer H, Cassidy J, Locke CA, Sigmundsson F (1998) Post-eruptive gravity changes from 1990 to 1996 at Krafla volcano, Iceland. *J Volcanol Geotherm Res* 87(1):141–149
- Siebert L, Simkin T, Kimberly P (2010) *Volcanoes of the world*, 3rd edn. University of California Press, Berkeley 568 p.
- Sturkell E, Sigmundsson F (2000) Continuous deflation of the Askja caldera, Iceland, during the 1983–1998 non eruptive period. *Journal of Geophysical Research: Solid Earth* (1978–2012) 105(B11):25671–25684
- Sturkell E, Einarsson P, Roberts MJ, Geirsson H, Gudmundsson M T, Sigmundsson F, Stefansson R (2008) Seismic and geodetic insights into magma accumulation at Katla subglacial volcano, Iceland: 1999 to 2005. *Journal of Geophysical Research: Solid Earth* (1978–2012) 113(B3)
- Sudo Y, Kong L (2001) Three-dimensional seismic velocity structure beneath Aso volcano Kyushu, Japan. *Bull Volcanol* 63:326–344
- Sudo Y, Tsutsui T, Nakaboh M, Yoshikawa M, Yoshikawa S, Inoue H (2006) Ground deformation and magma reservoir at Aso volcano: location of deflation source derived from long-term geodetic surveys. *Kazan* 51(5):291–309 In Japanese
- Takayama H, Yoshida A (2007) Crustal deformation in Kyushu derived from GEONET data. *J Geophys Res* 112(B6):B06413
- Tsutsui T, Sudo Y (2004) Seismic reflectors beneath the central cones of Aso volcano, Kyushu, Japan. *J Volcanol Geotherm Res* 131(1–2):33–58
- Unglert K, Savage MK, Fournier N, Ohkura T, Abe Y (2011) Shear wave splitting, vP/vS, and GPS during a time of enhanced activity at Aso caldera. *Kyushu J Geophys Res* 116:B11203. doi: [10.1029/2011JB008520](https://doi.org/10.1029/2011JB008520)
- Wang H, Wright TJ, Biggs J (2009) Interseismic slip rate of the north-western Xianshuihe fault from InSAR data. *Geophys Res Lett* 36: L03302. doi: [10.1029/2008GL036560](https://doi.org/10.1029/2008GL036560)
- Wang H, Wright TJ, Yu Y, Lin H, Jiang L, Li C, Qiu G (2012) InSAR reveals coastal subsidence in the Pearl River Delta, China. *Geophys J Int* 191:1119–1128. doi: [10.1111/j.1365-246X.2012.05687.x](https://doi.org/10.1111/j.1365-246X.2012.05687.x)
- Wright TJ, Lu Z, Wicks C (2003) Source model for the Mw 6.7, 23 October 2002, Nenana Mountain Earthquake (Alaska) from InSAR. *Geophys Res Lett* 30(18). DOI: [10.1029/2003GL018014](https://doi.org/10.1029/2003GL018014).
- Yang X, Davis PM, Dieterich JH (1988) Deformation from inflation of a dipping finite prolate spheroid in an elastic half-space as a model for volcanic stressing. *J Geophys Res* 93(B5):4289–4257